applied sciences

MDPI

Article

Reduction of Submicron-Sized Aerosols by Aerodynamically Assisted Electrical Attraction with Micron-Sized Aerosols

Hyun-Sik Choi and Jungho Hwang *

School of Mechanical Engineering, Yonsei University, 134 Sinchon-dong, Seodaemun-gu, Seoul 03722, Republic of Korea; hyuncs09@yonsei.ac.kr
* Correspondence: hwangjh@yonsei.ac.kr; Tel.: +82-2-2123-7226; Fax: +82-2-312-2821

Abstract: A vortex generator was installed inside an electric agglomeration device to apply aerodynamic agglomeration in the same space as electric agglomeration. Computational fluid dynamics simulation was utilized to assess the combined effects of electric and aerodynamic agglomeration, and this was subsequently validated through experiments. The discrete phase model was used to track particle trajectories. The results showed that both the aerodynamic agglomeration through the vortex generator and the electric agglomeration through the electric field were effective. When these two agglomerations existed individually in series, the total removal efficiency for submicron particles was 32.5%. However, when they coexisted in the same space, the efficiency increased to 50%. This increase is attributed to the increase in residence time when the vortex generator was added to a space with an electric field. This led to particles being exposed to the electric field for a longer duration, thus generating a synergistic effect.

Keywords: alternating current electric field; bipolarly charged; electric agglomeration; aerodynamic agglomeration; vortex generator

Citation: Choi, H.-S.; Hwang, J. Reduction of Submicron-Sized Aerosols by Aerodynamically Assisted Electrical Attraction with Micron-Sized Aerosols. *Appl. Sci.* **2024**, *14*, 10412. https://doi.org/10.3390/app142210412

Academic Editor: Domenico Lombardo

Received: 14 October 2024
Revised: 6 November 2024
Accepted: 8 November 2024
Published: 12 November 2024

1. Introduction

Submicron-sized particles suspended in air (aerosols) are hazardous as they can cause more adverse effects compared to larger particles [1]. Therefore, studying pretreatment technologies for removing submicron-sized particles is important [2]. In a conventional electrostatic precipitator (ESP), all particles are first charged by unipolar ions and then moved toward the collecting electrodes.

Agglomeration is an effective method to improve ESP collection efficiency, as smaller particles either are swept and scavenged by larger particles or form larger particles via agglomeration.

Unipolar charged aerosol agglomeration induces charging with a single polarity, causing relative movement due to differences in particle size and mass. Several studies including Hautanen et al. [3] and Kim et al. [4] have investigated the effect of unipolar charged particle agglomeration. Bipolar charged aerosol agglomeration, another method of electric agglomeration, operates on the principle that half of the particles in an air flow are positively charged in a corona charger, while the other half are negatively charged in another corona charger. These oppositely charged particles enter the agglomerator together and oscillate in an alternating current (AC) electric field [5,6]. Several studies have investigated the effect of bipolar charged particle agglomeration in an AC electric field, such as those by Jaworek et al. [5], Sobczyk et al. [7], Lehtinen et al. [8], Laitinen et al. [9], Kildeso et al. [10], and Ji et al. [11]. Recently, Choi and Hwang [12] reported a 25–27% decrease in the mass concentration of NaCl aerosols (100 nm) by attaching them to Arizona test dust 4 particles (1 μm) flowing together with the NaCl particles when an alternating current (AC; 10 kV/cm, 60 Hz) was applied to the agglomerator (the face velocity was 0.1 m/s, resulting in a residence time of 3 s). This decrease was in good agreement with

the one theoretically obtained from an agglomeration model. In the work of Choi and Hwang [12], the concentration and size of NaCl after a certain period of time (3 s) were derived from the initial concentration and size.

Aerodynamic agglomeration, also known as turbulent agglomeration, has been extensively studied to improve the removal of PM2.5 (particulate matter smaller than 2.5 μm) suspended in gas. In the study by Bin et al. [2], vortex generators were evenly arranged in an agglomeration chamber (face velocity = 15 m/s, residence time ≈ 0.1 s, flue gas flow rate = 350 m^3/h) installed at the inlet of an ESP. The number concentration of PM2.5 at the inlet of the agglomeration chamber was 1.93 × 10^7 particles/cm^3, which decreased to 1.44 × 10^7 particles/cm^3 at the outlet of the agglomeration chamber (25.4% decrease). Sun et al. [13] studied aerodynamic agglomeration to promote the removal of PM10 aerosols. Their aerodynamic agglomerator had a square cross-section with eight pairs of vortex generators alternately arranged in two columns. The PM10 number concentration was approximately 9.08 × 10^6 particles/cm^3 in the original flue gas, which reduced to 7.69 × 10^6 particles/cm^3 after turbulent agglomeration (15.4% decrease). The gas velocity was 10 m/s and the gas flow rate was 300 m^3/h (residence time ≈ 0.3 s). Chen et al. [14] installed two aerodynamic agglomerators (flue gas velocity = 15.2 m/s, gas flow rate = 350 m^3/h, residence time ≈ 0.18 s) in front of the electrostatic precipitator of a 330 MW PC-fired boiler. The PM2.5 and PM10 particles were swept and scavenged by 50–100 μm particles, resulting in mass concentration decreases of 56.2% and 50.6% for PM2.5 and PM10 particles, respectively. Liu et al. [15] investigated the structural characteristics of vortex generators affecting particle agglomeration. Triangular vortex generators were used for turbulent flow. At a flow velocity of 4.8 m/s (residence time ≈ 0.3 s), the removal efficiency for particles of 15.7–850 nm was approximately 16.42%. Crynack et al. [16] and Truce et al. [17] researched a technology called Indigo Agglomeration. The Indigo Agglomerator was placed at the inlet duct right before the electrostatic precipitator. Fine particles that entered the Indigo Agglomerator became attached to larger particles through a mix of electrostatic and fluidic mechanisms.

In this study, aerodynamic agglomeration was combined with electric agglomeration in same space to improve the removal efficiency of submicron-sized aerosols. A vortex generator was installed inside the electric agglomeration device used in our previous study, by Choi and Hwang [12], so that aerodynamic agglomeration was additionally applied to the electric agglomeration in the same space.

In addition to experiments, numerical calculations were performed using the population balance equation (PBE) model, which has been used to track changes in the number density function (or particle size distribution) due to different mechanisms, including agglomeration [18]. The PBE was employed through FLUENT, a commercial computational fluid dynamics (CFD) package, to derive both electric and turbulent agglomeration constant values basis changes in particle size and concentration at each moment.

2. Theory

The rate of change of number concentration in particles suspended in stagnant air caused by particle agglomeration can be expressed as follows:

$$\frac{dN_i}{dt} = -K_i {N_i}^2 \quad (1)$$

where N_i denotes the number concentration of the particle (of size d_i) and K_i is the agglomeration coefficient defined as the effective particle collision volume per second.

As the actual particles are mostly polydisperse particles, the agglomeration coefficient can be obtained by the following equation:

$$K_i = \sum_{j=1}^{n} K_{ij} f_i f_j \quad (2)$$

The fraction of concentration, f_i, is defined as follows:

$$f_i = \frac{N_i}{N_{total}} \tag{3}$$

where N_{total} denotes the total concentration of all particles and K_{ij} is the agglomeration coefficient between a particle of diameter d_i and a particle of diameter d_j.

Koizumi et al. [19] determined the agglomeration coefficient for bipolar charged particles of various sizes. Their model, based on the equation of motion of a charged single particle, calculated particle trajectories using DC/AC electric fields as key variables. The results indicated that the AC electric field had a more significant coagulation effect compared to the DC electric field. Additionally, Tan et al. [20] developed an approximate formula for the agglomeration coefficient of bipolar charged particles under an AC electric field. According to Tan et al. [20], K_{CF-ij} is the agglomeration coefficient of bipolar charged particles by the Coulomb force without the effect of an external electric field between particles of diameters d_i and d_j:

$$K_{ij} = K_{CF\ ij} = \frac{q_i q_j (d_i + d_j)}{3\pi\varepsilon_0 \mu d_i d_j} \tag{4}$$

where μ is the air viscosity and ε_0 is the permittivity of free space. The charging quantity of i-th particle, q_i, is

$$q_i = n_i e \tag{5}$$

where e is the elementary unit of charge (1.6×10^{-19} C). The charge number of i-particle, n_i, can be calculated using the following equation:

$$n_i = \frac{d_i \mathrm{k} T}{2\mathrm{K_E} e^2} \ln\left[1 + \frac{\pi \mathrm{K_E} d_i \bar{\mathrm{c}}_\mathrm{i} e^2 N_{ion} t_c}{2\mathrm{k}T}\right] + \left(\frac{3\varepsilon_R}{\varepsilon_R + 2}\right)\left(\frac{E {d_i}^2}{4\mathrm{K_E} e}\right)\left(\frac{\pi \mathrm{K_E} e Z_{ion} N_{ion} t_c}{1 + \pi \mathrm{K_E} e Z_{ion} N_{ion} t_c}\right) \tag{6}$$

where k denotes the Boltzmann constant (~1.38×10^{-23} J/K), T is the temperature, $\mathrm{K_E}$ is the electrostatic constant of proportionality (9×10^9 $\mathrm{Nm^2/C^2}$), $\bar{c}_{ion}$ is the mean thermal speed of the ions (240 m/s) at standard condition, Z_{ion} is the electrical mobility of an ion (1.5×10^{-5} $\mathrm{m^2/V{\cdot}s}$), N_{ion} is the ion number concentration, t_c is the time passing through the charger, and ε_R is the relative permittivity of the particle. According to Tan et al. [20], the agglomeration coefficient of bipolar charged particles by the alternating current electric field without the effect of the Coulomb force is as follows:

$$K_{ij} = K_{EF\ ij} = \frac{\left(d_i + d_j + 2Y_{AC}\right)^2}{6\pi\mu} E_{AC}\left(\frac{q_i}{d_i} C_{Ci} + \frac{q_j}{d_j} C_{Cj}\right) \tag{7}$$

where E_{AC} is the alternating electric field. Y_{AC}, which is the distance between the particles, can be approximated using the following equation:

$$Y_{AC} = \sqrt[3]{\mathrm{C_5} \frac{q_i q_j}{4\pi^2 \mu \varepsilon_0 (X_i + X_j)} \left(\frac{C_{Ci}}{d_i} + \frac{C_{Cj}}{d_j}\right)} \tag{8}$$

where C_{Ci} is the Cunningham slip correction coefficient of i-particle, $C_5 \approx 0.5 \times 10^{-8}$ (dimensionless). Tan et al. [20] proposed an approximate expression for the agglomeration coefficient of bipolar charged particles with the effect of an AC electric field.

$$K_{ij} = K_{EF+CF\ ij} = \frac{q_i q_j (d_i + d_j)}{3\pi\varepsilon_0 \mu d_i d_j} + \frac{\left(d_i + d_j + 2Y_{AC}\right)^2}{6\pi\mu} E_{AC}\left(\frac{q_i}{d_i} C_{Ci} + \frac{q_j}{d_j} C_{Cj}\right) \tag{9}$$

When particles drift together with air flow velocity $\vec{u}$, the rate of change of particle number concentration can be expressed as follows:

$$\frac{dN_i}{dt} + \nabla \cdot \vec{u} N_i = -K_i {N_i}^2 \tag{10}$$

In the case of aerodynamic (turbulent) agglomeration, Saffman and Turner [21] proposed the following approximate expression for the agglomeration coefficient of two particles with the effect of an aerodynamic collision:

$$K_{ij} = K_{AF\ ij} = \beta \sqrt{\frac{8\pi}{15}} \gamma \frac{(d_i + d_j)^3}{8} \tag{11}$$

where β is a pre-factor that takes into account the capture efficiency coefficient of aerodynamic collision (dimensionless), and γ is the shear rate (s^{-1}):

$$\gamma = \frac{\rho \epsilon^{0.5}}{\mu} \tag{12}$$

where ρ is the air density (kg/m^3), ϵ is the turbulent energy dissipation rate (m^2/s^3). Higashitani et al. [22] proposed the following relation:

$$\beta = 0.732 \left(\frac{5}{N_T}\right)^{0.242} \tag{13}$$

where N_T is the ratio between the viscous force and the Van der Waals force,

$$N_T = \frac{6\pi\mu\alpha(d_i + d_j)^3}{8H} \tag{14}$$

where H is the Hamaker constant, a function of the particle material, and α is the deformation rate (s^{-1}),

$$\alpha = \left(\frac{4\rho\epsilon}{15\pi\mu}\right)^{0.5} \tag{15}$$

Combining Equations (9) and (11), we can obtain the total agglomeration coefficient of bipolar charged particles by an external electric field with the effective Coulomb force and the aerodynamic effect.

$$K_{ij} = \frac{q_i q_j (d_i + d_j)}{3\pi\varepsilon_0 \mu d_i d_j} + \frac{(d_i + d_j + 2Y_{AC})^2}{6\pi\mu} E_{AC} \left(\frac{q_i}{d_i} C_{Ci} + \frac{q_j}{d_j} C_{Cj}\right) + \beta \sqrt{\frac{8\pi}{15}} \gamma \frac{(d_i + d_j)^3}{8} \tag{16}$$

3. Numerical

Mathematically, a multidimensional agglomeration population balance equation (PBE) can be expressed in terms of an integro-partial differential equation as follows:

$$\frac{\partial n(v)}{\partial t} + \nabla \cdot (\vec{u} n(v)) = B(v) - D(v) \tag{17}$$

where $n(v)$ is the number density function, v is the volume of a particle, and $\vec{u}$ is the gas flow velocity vector. $B(v)$ and $D(v)$ denote the birth and death rates of particles of volume v, respectively:

$$B(v) = \frac{1}{2} \int_0^v K_{ij}(v - v', v') n(v - v') n(v) dv' \tag{18}$$

$$D(v) = \int_0^\infty K_{ij}(v, v') n(v') n(v) dv' \tag{19}$$

where v' is the volume of another particle with a different size. K_{ij} refers to the total agglomeration coefficient of bipolar charged particles by an external electric field with the effective Coulomb force and with the aerodynamic effect (see Equation (16)). The gas flow velocity $\vec{u}$ was determined by solving the continuity and Navier–Stokes equations. The standard k-ε turbulence model was utilized.

Details of governing equations are presented as follows:

$$\text{Continuity } \frac{\partial}{\partial t}(\rho) + \nabla \cdot \left(\rho \vec{u}\right) = \vec{S} \tag{20}$$

$$\text{Momentum } \frac{\partial}{\partial t}\left(\rho \vec{u}\right) + \nabla\left(\rho \vec{u}\,\vec{u}\right) = -\nabla p + \mu \nabla^2 \vec{u} + \rho \vec{g} \tag{21}$$

$$\text{Turbulence k } \frac{\partial}{\partial t}(\rho k) + \frac{\partial}{\partial x_i}\left(\rho k \vec{u}\right) = \frac{\partial}{\partial x_j}\left[\left(\mu + \frac{\mu_t}{\sigma_k}\right)\frac{\partial k}{\partial x_j}\right] + P_k - \rho\epsilon \tag{22}$$

$$\text{Turbulence } \epsilon \frac{\partial}{\partial t}(\rho\epsilon) + \frac{\partial}{\partial x_i}\left(\rho\epsilon \vec{u}\right) = \frac{\partial}{\partial x_i}\left[\left(\mu + \frac{\mu_t}{\sigma_k}\right)\frac{\partial \epsilon}{\partial x_i}\right] + C_{1\epsilon}\frac{\epsilon}{k}P_k - C_{2\epsilon}\rho\frac{\epsilon^2}{k} \tag{23}$$

where $\vec{S}$ is the source term, p is the static pressure, and $\vec{g}$ is the gravitational acceleration. P_k is the generation of turbulent kinetic energy due to the mean velocity gradients, and ϵ is the dissipation rate of the turbulent energy. $C_{1\epsilon}$ = 1.44 and $C_{2\epsilon}$ =1.92 are model constants. The boundary conditions are presented in Table 1.

Table 1. Boundary conditions.

Position	Velocity [m/s]	Pressure [Pa]	Condition
Inlet	0.1	$\frac{\partial P}{\partial n} = 0$	Escape
Wall	-	-	Trap
Outlet	0	$P = P_{atm}$	Escape

In this study, numerical calculations were performed for a domain of the lab-scale agglomerator (see Figure 1a, with a cross-sectional area of 4 × 4 cm^2 and a length of 0.6 m). The CFD grids were generated via ANSYS meshing, with a total grid number of approximately one million. The inlet air speed was set at 0.1 m/s, and the outlet was set at atmospheric pressure. In accordance with the particle distribution used in the experiment, the minimum size of the inlet particles was set to 50 nm and the maximum particle size was set to 8.2 μm. There were 49 different sizes between 50 nm and 8.2 μm, resulting in a polydisperse distribution. The total concentration was 3.58 × 10^6 particles per cm^3 of air. The time step was set to 0.01 s, the number of time steps was 300, and the number of iterations per time step was 50.

In addition, the discrete phase model (DPM) was employed to observe the trajectories of different particles. The equation of motion of a single particle is as follows:

$$m\frac{d\vec{u}_p}{dt} = m\frac{\left(\vec{u} - \vec{u}_p\right)}{\tau_r} + m\frac{\vec{g}\left(\rho_p - \rho\right)}{\rho_p} \tag{24}$$

where τ_r is the particle relaxation time given as

$$\tau_r = \frac{{d_p}^2 \rho_p C_C}{18\mu} \tag{25}$$

where $\vec{u}_p$ is the particle velocity, m is the particle mass, d_p is the particle diameter, and ρ_p is the particle density, respectively. Through Equation (24), the velocity can be derived, and the particle's position can be calculated through integration of the velocity,

$$x_{\mathrm{p}}^{n+1} = x_{\mathrm{p}}^{n} + \int_{n}^{n+1} \overrightarrow{u_p^{n+1}}\, dt \ (n \geq 0) \tag{26}$$

where $\vec{x_p}$ is the position of the particle and n is the time step.

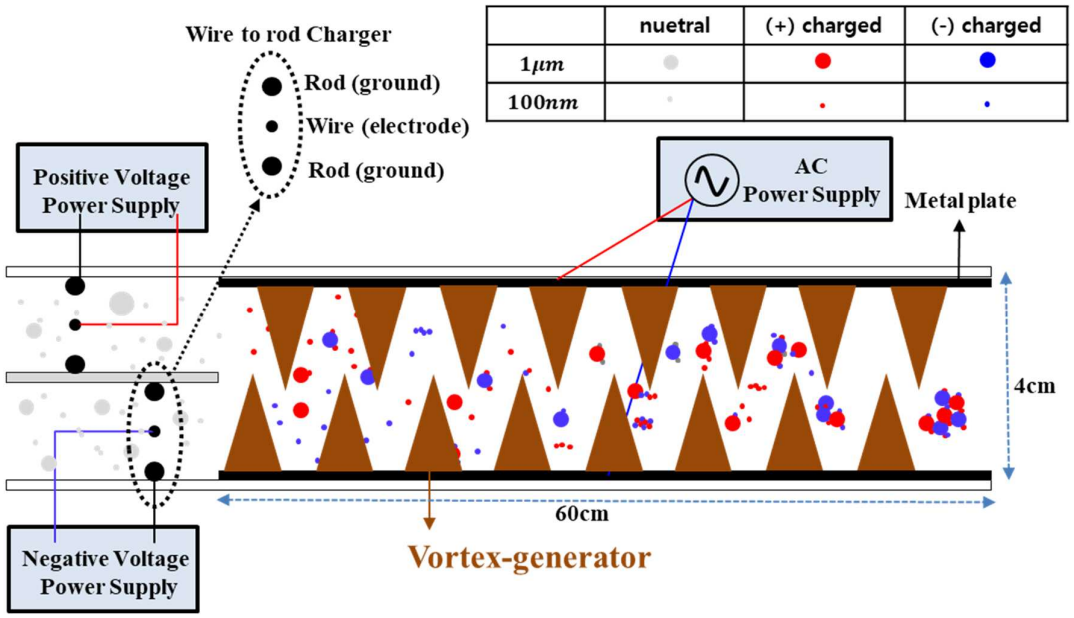

(**a**)

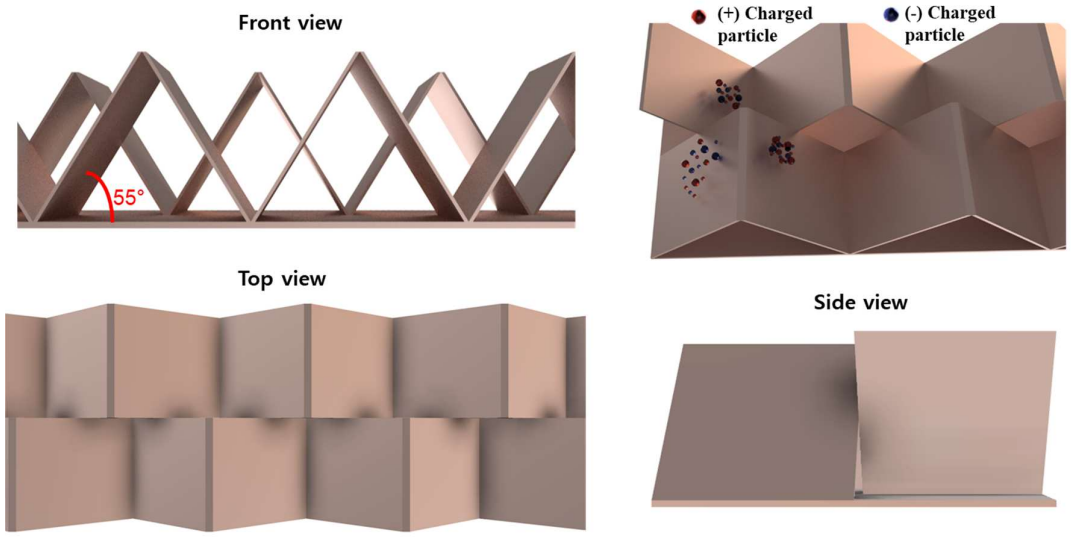

(**b**)

Figure 1. (**a**) Conceptual schematic of aerodynamically assisted electric agglomeration, (**b**) 3D geometry of the vortex generator.

4. Experiment

The conceptual schematic of this study is explained in Figure 1a. Uncharged 100 nm particles at a concentration of 10^7 particles per cm^3 air (selected as an example of submicron-sized particles) and 1 μm particles at a concentration of 10^4 particles per cm^3 air (selected as

an example of micron-sized particles) with air flow were injected into the wire (electrode) to rod (ground) type charger. Half of this particle mixture was positively charged (red) while the other half was negatively charged (blue) before entering the agglomerator. In the agglomerator, larger particles oscillated at higher amplitudes due to their higher charge number acquired when passing through the charger, sweeping smaller particles and leading them to attach to the larger particles. Additionally, the vortex generated by the vortex generator installed in the agglomerator increased the collision probability of particles, enhancing the agglomeration efficiency and reducing the number concentration of smaller particles. Smaller particles are more likely to collide with larger ones because their relative velocity is greater compared to particles of similar size (Alves et al. [23]). The vortex generator consisted of thin plates arranged repeatedly in an isosceles triangle shape (see Figure 1b).

Figure 2 shows the experimental setup, mainly composed of (a) the test particle generation part, (b) the particle charging/agglomeration part, and (c) the measuring part. In Figure 2a, compressed air, used as a carrier gas, was purified by passing through a clean-air supply system designed to remove oil droplets, moisture, and contaminants. This clean-air supply system included an oil trap, a diffusion dryer, and a high-efficiency particulate air (HEPA) filter. The purified air entered the particle generation device through a mass flow controller (MFC). Nano-sized NaCl particles were generated using the evaporation-condensation method with a tube furnace. Arizona test dust 4 (A4; micro-sized) particles were generated using a solid aerosol generator (SAG410, TOPAS, Dresden, Germany). In the SAG, a moving toothed belt continuously supplied test dust particles dispersed from the belt by compressed air.

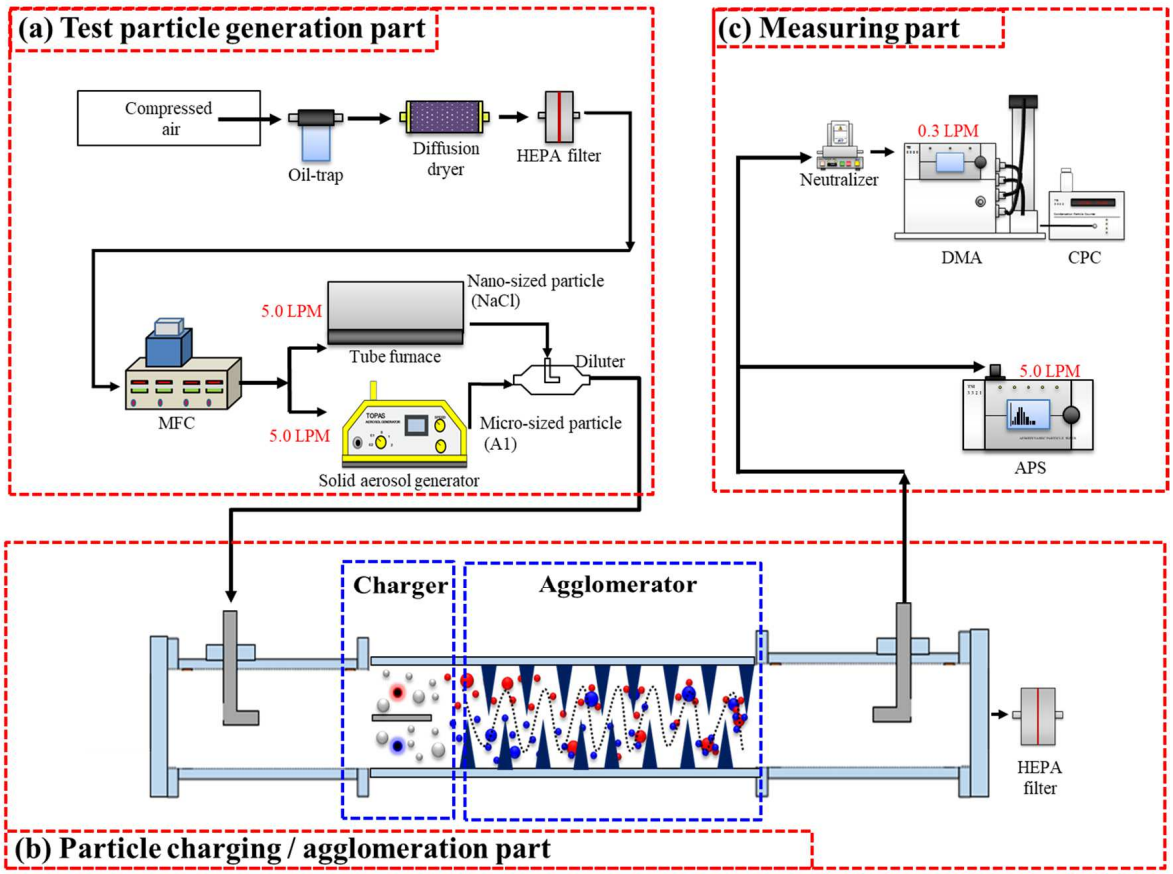

Figure 2. Experimental setup: (**a**) test particle generation part, (**b**) particle charging/agglomeration part, and (**c**) measuring part.

In Figure 2b, the air flow containing both the NaCl particles and A4 particles passed through the charger with a face velocity of 0.1 m/s. Two corona chargers were located in the charging part in parallel, with DC voltages of +6 kV and −6 kV applied to the chargers, respectively. Each charger consisted of a wire (diameter: 0.1 mm) and two grounded rods (diameter: 2 mm). The distance between the wire and the grounded rod was 7.95 mm. An AC high-voltage power supply with a peak-to-peak voltage of ±20 kV was used, resulting in a field strength of 3.5 kV/cm (rms). The frequency of the AC power supply was 60 Hz. The agglomerator comprised two parallel metal plates placed 4 cm apart and a vortex generator (made of acrylic, length: 60 cm, cross-sectional area: 4×4 cm^2). The vortex generator comprised thin plates (width: 4.8×2 cm^2; thickness: 1.6 mm) arranged repeatedly in an isosceles triangle shape of 55° (see Figure 1b). Between two triangle shapes of 55° and 70°, the shape of 55° was chosen since this shape could cause a lower pressure drop. Details are presented in Section S1 of the Supplementary Materials.

After the agglomeration, a portion of the particle flow was delivered to the measuring part (see Figure 2c). The particle size distribution was determined using both a scanning mobility particle sizer (SMPS) and an aerodynamic particle sizer (APS, 3321, TSI, Shoreview MN, USA). The APS employed optical sensors to measure the concentrations of particles with aerodynamic diameters ranging from 0.5 μm to 20 μm. The sampling flow rate of the APS was 5 L/min. The SMPS comprised a differential mobility analyzer (DMA, 3081, TSI, Shoreview MN, USA) and a condensation particle counter (CPC, 3776, TSI, Shoreview MN, USA). Prior to entering the DMA, the particles underwent Boltzmann charge distribution adjustment through a neutralizer (Soft X-ray Charger 4530, HCT, Icheon, Republic of Korea). In the DMA, particles with a charge number of +1 were classified based on their electrical mobility-based size according to the voltage change. The DMA classified particles ranging from a minimum size of 10 nm to approximately 800 nm, and the classified particles were quantified for their number concentration using a sensor in the CPC. The sampling flow rate was 0.3 L/min, and the scanning time was 120 s.

5. Results

In case of no electric field applied to the agglomerator, Figure 3a shows numerical calculation results for the front and top views of flow streamlines inside the agglomerator when the inlet air speed was 0.1 m/s. The front view shows that the flow upstream of the agglomerator is in a straight line with an average velocity of 0.1 m/s (light blue). However, the flow curves when it passes through the region of the vortex generator. At the same time, the flow is accelerated to speeds ranging from 0.2 to 0.4 m/s (light green to yellow). Furthermore, the flow becomes more complicated near the exit region, compared to its relatively straight behavior at the entrance region. As shown in the magnified image of the top view, where upward and downward movements of the flow are clearly visible, the presence of vortices is confirmed.

Figure 3b shows the contours of the turbulent energy dissipation rate in the agglomerator when the inlet air speed was 0.1 m/s. The turbulent energy dissipation rate was calculated using the standard k-ϵ turbulence model. The left-side contour shows a case of no vortex generator installed in the agglomerator, while the right-side contour represents a case of the vortex generator installed in the agglomerator. In the left-side contour, the turbulent energy dissipation rate is as low as 0.01 m^2/s^3, depicted in blue. However, in the right-side contour, the turbulent energy dissipation rate increases up to 1.5 m^2/s^3 inside the vortex generator region, depicted in various colors such as green, yellow, and red. This increase can be attributed to the increased agglomeration efficacy, as explained in Equation (6).

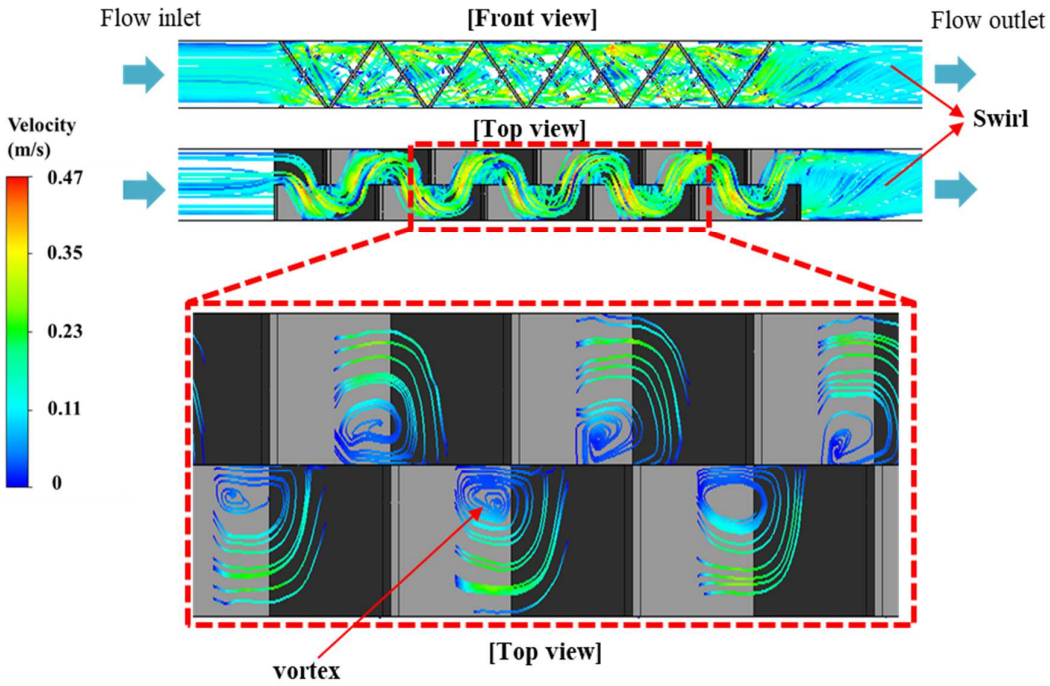

(**a**)

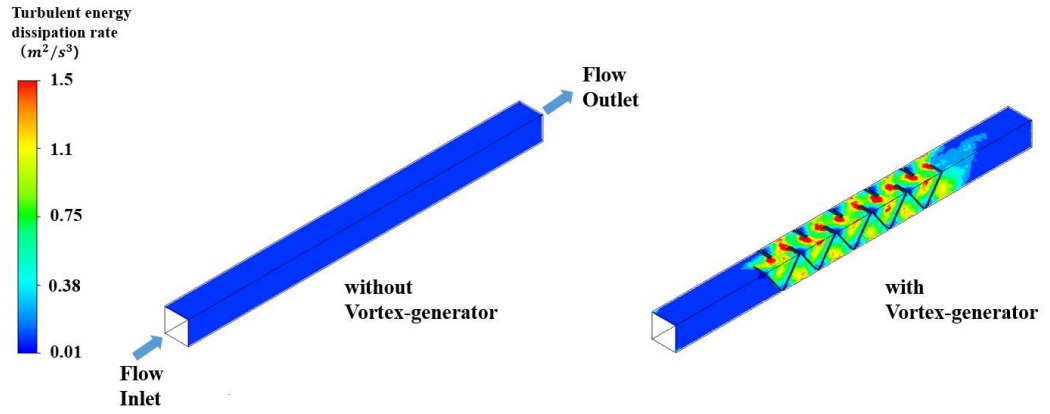

(**b**)

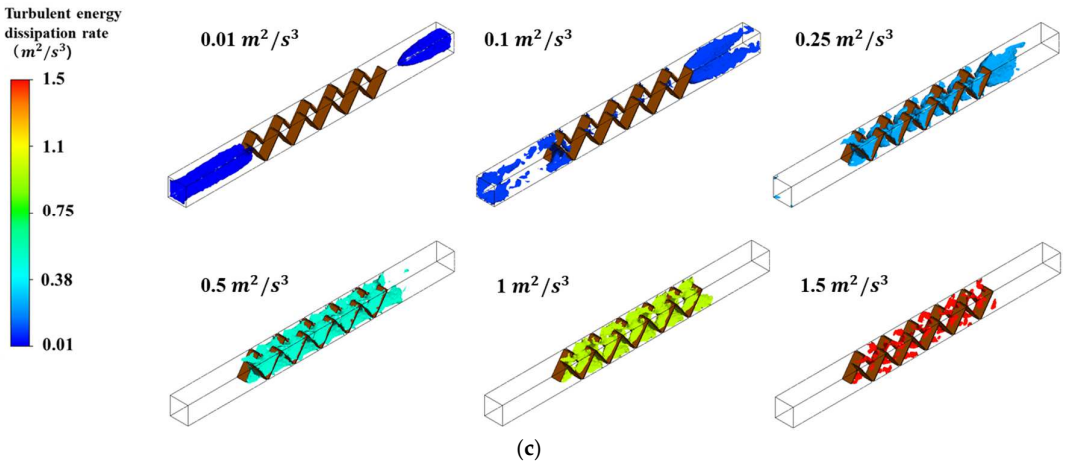

(**c**)

Figure 3. (**a**) Flow fields in the vortex generator in the absence of an electric field, (**b**) surface contours of turbulent energy dissipation rate, (**c**) six iso-surfaces of turbulent energy dissipation rate.

The turbulent energy dissipation rate values shown in the right-side contour of Figure 3b are separated into six different values: 0.01, 0.1, 0.25, 0.5, 1, and 1.5 m^2/s^3. Each value is represented in a contour in Figure 3c. The values of 0.01 and 0.1 m^2/s^3 are represented in blue at the inlet and outlet regions of the vortex generator. The values from 0.25 m^2/s^3 to a maximum of 1.5 m^2/s^3 are distinctly observable inside the regions near the vortex generator.

Figure 4 presents the current/voltage characteristics of the corona chargers used in our study. The corona currents were measured at various applied voltages, showing that the current gradually increased once the corona onset voltage was exceeded. It was observed that the current for negative voltage was higher than for positive voltage of the same magnitude, which was a phenomenon also noted by Wang, L. K. [24]. Since corona current is proportional to air ion concentration, the negative discharge produced more air ions compared to the positive discharge. At applied voltages of (+) 6 kV and (−) 6 kV, the measured currents were (+) 1.32 μA and (−) 3.51 μA, respectively.

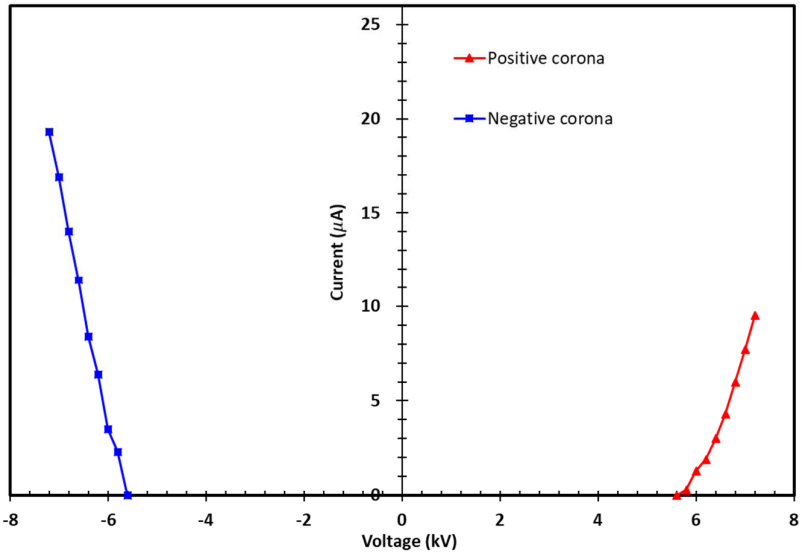

Figure 4. Current–voltage characteristics.

Particle size distributions were measured both upstream and downstream of the agglomerator in which the vortex generator was placed. The electric field was not applied to the agglomerator (see Figure 5a). For the measurement, NaCl (count mean diameter, CMD; 100 nm) and Arizona test dust (count mean diameter, CMD; 1 μm) were generated, as explained in Section 4, and delivered to the agglomerator. The results for submicron particles are shown in Figure 5b. The solid orange line represents the upstream distribution of submicron particles (NaCl) generated through experiments, while the solid black line indicates the downstream distribution measured after passing through the vortex generator. The total number concentration that was obtained by integration of a size distribution function was 3.69×10^6 particles per cm^3 of air volume upstream but decreased to 3.45×10^6 particles per cm^3 of air volume (6.5% decrease) downstream. The observed 6.5% decrease agreed with an 8% decrease (numerical calculation, see black dotted line).

To investigate wall losses, the DPM was utilized to determine the trajectories of submicron particles and the corresponding wall losses. A total of 200 particles were introduced, of which 3 particles were captured by the wall, resulting in a wall loss of 1.5%. Details are presented in Section S2 of the Supplementary Materials.

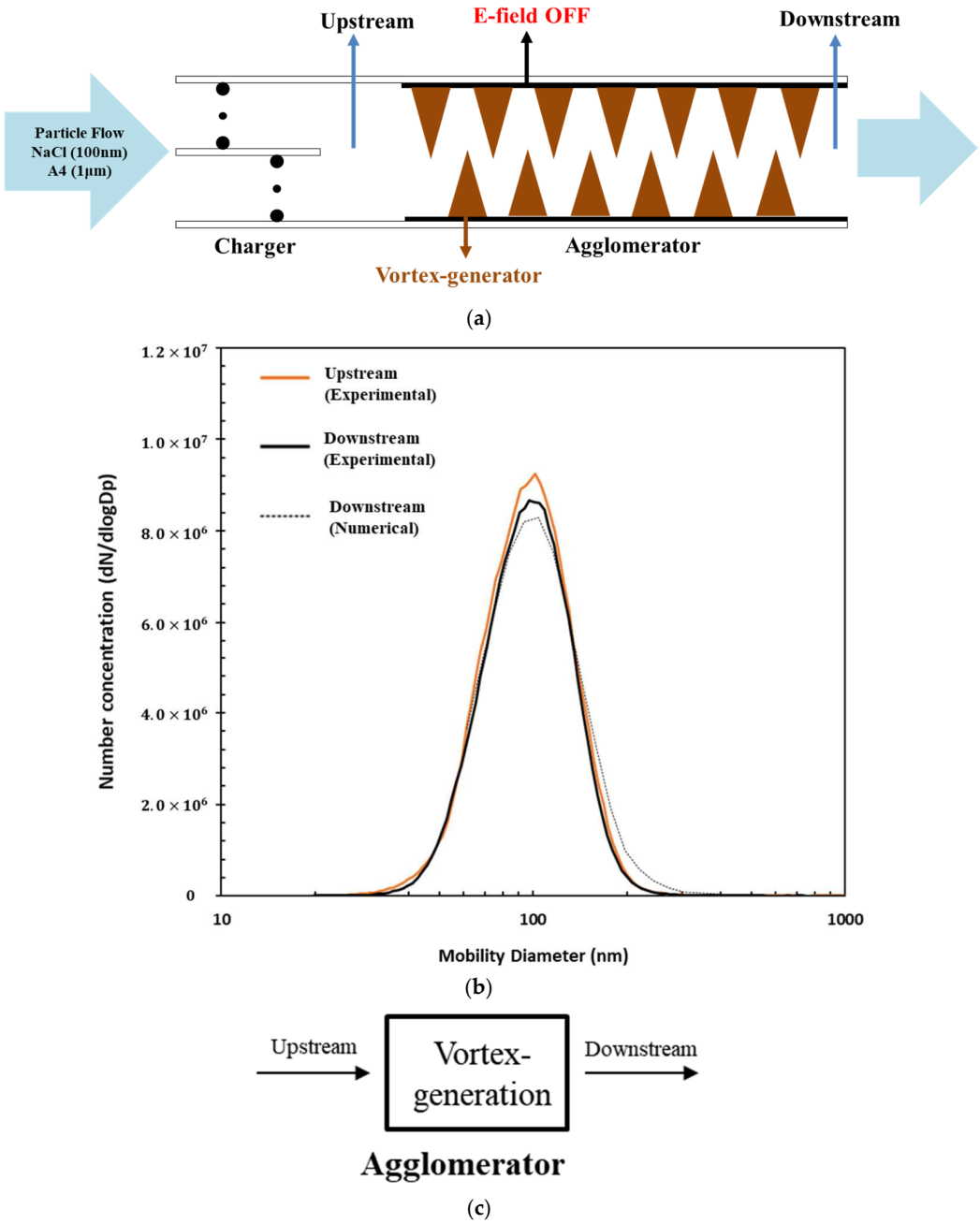

Figure 5. (**a**) Overview: without an electric field applied to the agglomerator, (**b**) particle size distributions upstream and downstream of the agglomerator, (**c**) vortex generation as an agglomeration factor.

Therefore, the decrease in the number concentration of submicron particles shown in Figure 5b is believed to be a result of particle agglomeration induced by the vortices generated when the flow passed through the vortex generator. In other words, submicron particles are swept and scavenged by larger particles (micron particles). The results of Figure 5b can be simplified using the relation between upstream and downstream number concentrations of submicron particles (Figure 5c) as follows:

$$N_{Down} = (1 - \eta_{VG})N_{Up} \quad (27)$$

where N_{Down} is the downstream submicron particle concentration (3.45×10^6 particles per cm^3 of air volume), N_{Up} is the upstream submicron particle concentration (3.69×10^6 par-

ticles per cm^3 of air volume), and η_{VG} is the submicron particle reduction efficiency in passing through the vortex generator (=0.065).

Size distributions of submicron particles were also obtained both upstream and downstream of the agglomerator when the AC electric field was applied to the agglomerator (see Figure 6a). The results in Figure 6b show that the total number concentration downstream decreased to 1.87×10^6 particles per cm^3 of air volume (measured) from the upstream concentration of 3.69×10^6 particles per cm^3 of air volume when the AC electric field was applied. The observed 50% decrease agreed with a 46% decrease (numerical calculation, see black dotted line). Therefore, the decrease in the number concentration is believed to be a result of particle agglomeration induced by the electric field when the flow passed through the vortex generator. When an electric field was applied, a relatively greater number of particles were reduced.

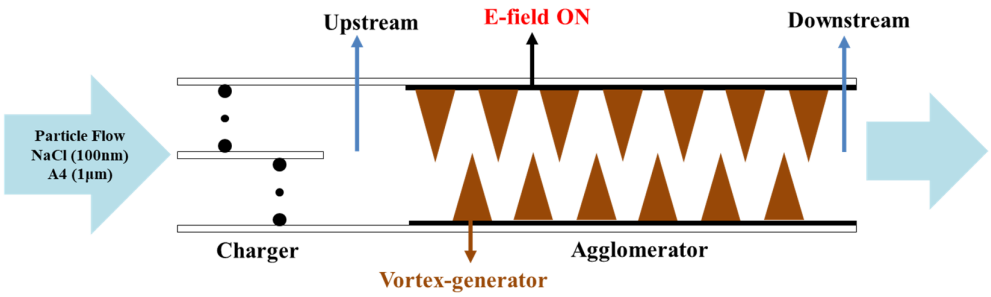

(**a**)

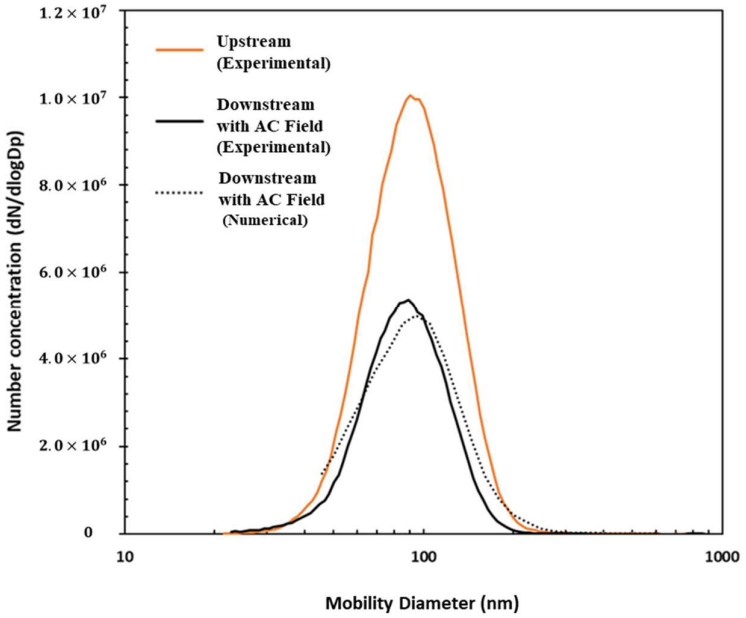

(**b**)

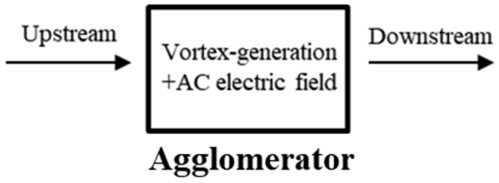

(**c**)

Figure 6. (**a**) Overview: with an electric field applied to the agglomerator, (**b**) particle size distributions upstream and downstream of the agglomerator, (**c**) vortex generation combined with AC electric field as an agglomeration factor.

The results of Figure 6b can be simplified using the relation between upstream and downstream number concentrations (Figure 6c) as follows:

$$N_{Down} = (1 - \eta_{VG+E})N_{Up} \tag{28}$$

where N_{Down} is the downstream particle concentration (1.87×10^6 particles per cm^3 of air volume) and N_{Up} is the upstream particle concentration (3.69×10^6 particles per cm^3 of air volume). η_{VG+E} is the particle reduction efficiency in passing through the vortex generator in which an electric field is applied (=0.5).

6. Discussion

When considering the agglomerator with a vortex generator but no electric field (see Figure 5a) and the electric agglomerator without the vortex generator (see Figure 7a), the overall efficiency of a system consisting of these two agglomerators arranged in series is given by the following equation:

$$\eta_{overall} = 1 - (1 - \eta_{VG})(1 - \eta_E) \tag{29}$$

where η_E is the particle reduction efficiency in passing through the electric agglomerator (without the vortex generator). The number concentration at a position downstream of the system is represented as follows:

$$N_{Down} = (1 - \eta_{VG})(1 - \eta_E)N_{Up} \approx \{1 - (\eta_{VG} + \eta_E)\}N_{Up} \tag{30}$$

To determine whether the particles were significantly reduced purely by the electric field (i.e., to determine η_E), additional experiments were performed when the vortex generator was removed from the agglomerator where the electric field was applied (Figure 6a). The results are shown in Figure 7b. When the vortex generator was absent (Figure 7a), the number concentration at a position downstream decreased to 2.71×10^6 particles per cm^3 of air volume from the upstream concentration of 3.69×10^6 particles per cm^3 of air volume (26% decrease, η_E = 0.26). The results of Figure 7b can be simplified using the relation between upstream and downstream number concentrations (Figure 7c):

$$N_{Down} = (1 - \eta_E)N_{Up} \tag{31}$$

η_{VG+E} (=0.5) is greater than $\eta_{VG} + \eta_E$ (=0.065 + 0.26 = 0.325). Additional CFD simulation was performed to investigate the cause of the difference between η_{VG+E} and $\eta_{VG} + \eta_E$. In the simulation, the DPM was employed to calculate trajectories of different particles. Figure 8a illustrates positions of a representative single particle at different times inside the agglomerator without a vortex generator installed. It takes 2.33 s for the particle to pass through the agglomerator from the inlet to the outlet. Meanwhile, Figure 8b illustrates positions of a particle at different times inside the agglomerator with a vortex generator installed. The time required for the particle to pass through the agglomerator is 6.13 s. This increase in residence time by 2.33 s ensures more chances of exposure to the electric field. Therefore, the application of an electric field to a space where a vortex generator is located results in an efficiency of η_{VG+E}, which is higher than the summation of two individual efficiencies, $\eta_{VG} + \eta_E$. Huang et al. [25] also reported an extension of residence time for fine particles and an increase in dust collection efficiency by installing a vortex generator. The increase in residence time when the vortex generator was added to the space in which an electric field was applied led particles to be exposed to the electric field for a longer duration, thus generating a synergistic effect.

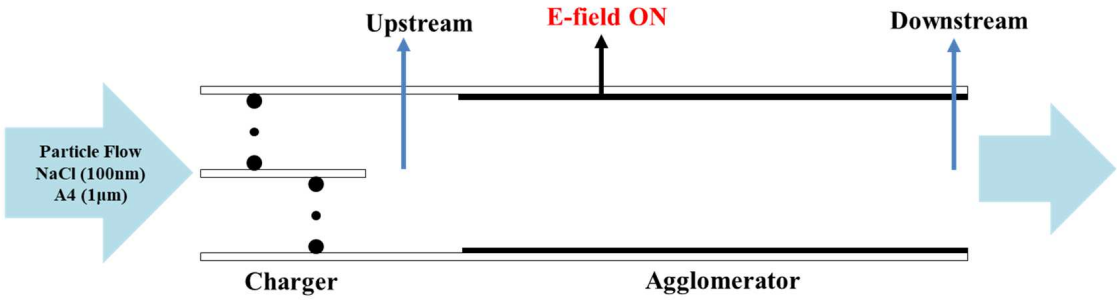

(**a**)

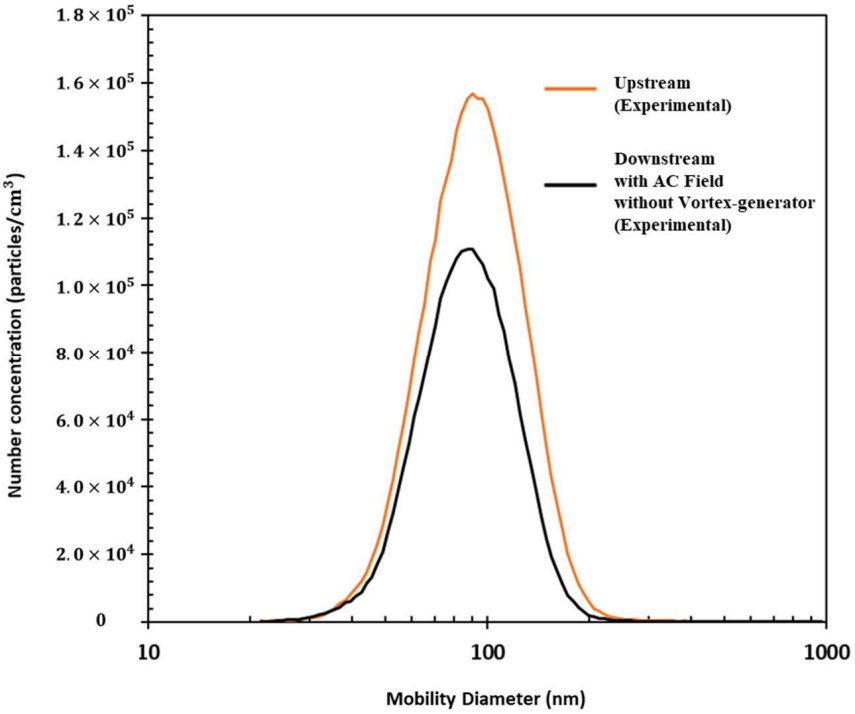

(**b**)

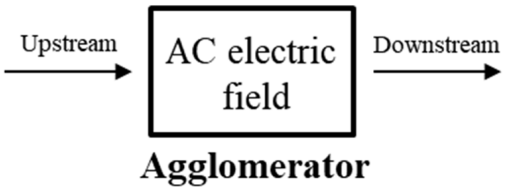

(**c**)

Figure 7. (**a**) Overview: with an electric field applied to the agglomerator (without a vortex generator), (**b**) particle size distributions upstream and downstream of the agglomerator, (**c**) AC electric field as an agglomeration factor.

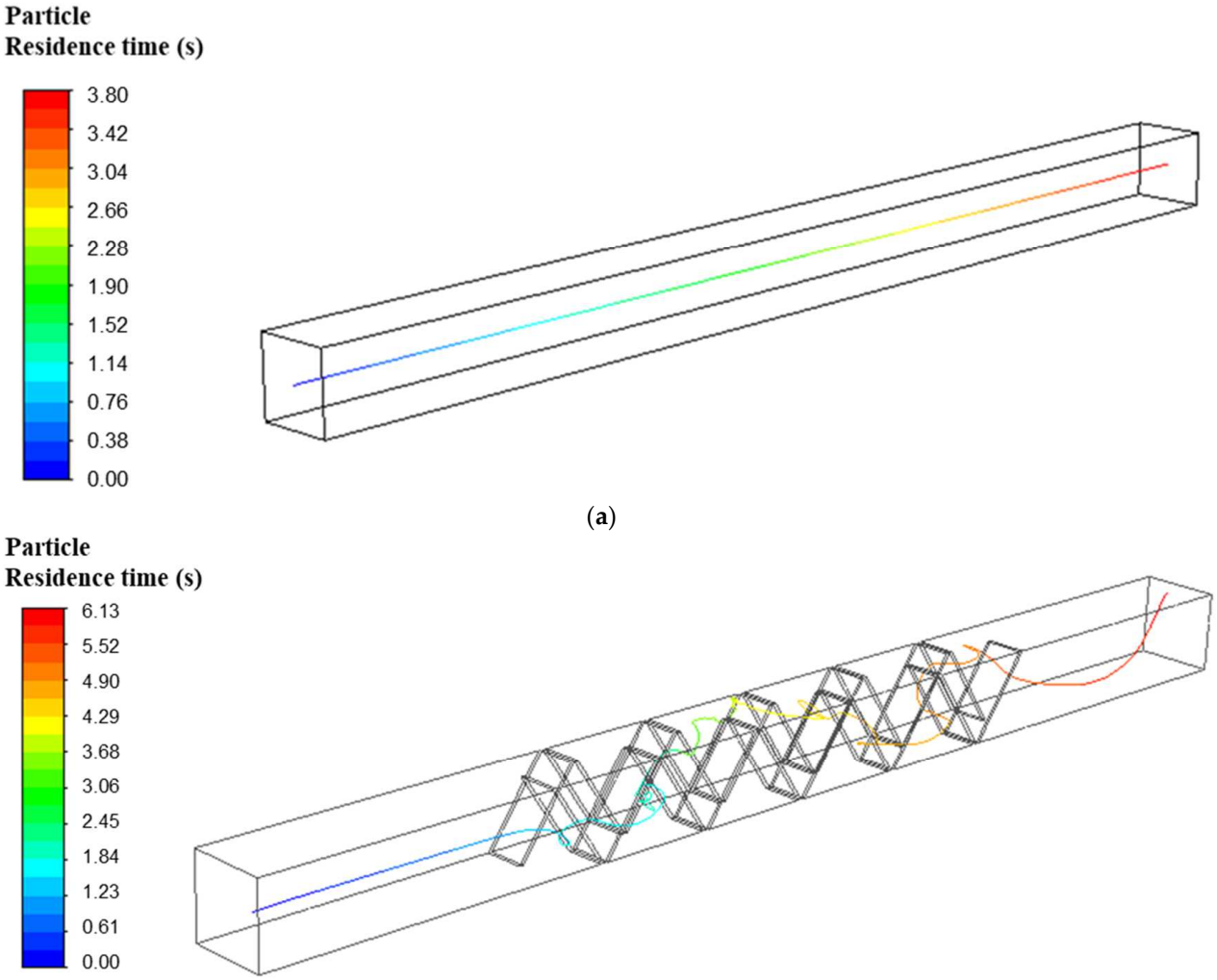

Figure 8. (**a**) Locations of a single particle at different times in the agglomerator without the vortex generator, (**b**) locations of a single particle at different times in the agglomerator with a vortex generator.

7. Conclusions

This study demonstrated the distribution of submicron particles after aerodynamic and electric agglomerations in terms of nanoparticle removal. The presence of the vortex generator increased the turbulent energy dissipation rate by up to 1.5 m^2/s^3, leading to an increase in the aerodynamic coefficient and particle residence time. When these two agglomerations existed individually in series, the total removal efficiency for submicron particles was 32.5%. However, when they coexisted in the same space, the efficiency increased to 50%. This increase is attributed to the increase in residence time when the vortex generator was added to a space with an electric field. This led to particles being exposed to the electric field for a longer duration, thus generating a synergistic effect.

Supplementary Materials: The following supporting information can be downloaded at https://www.mdpi.com/article/10.3390/app142210412/s1, Section S1: Comparison between vortex generator shapes (numerical calculation), Section S2: Trajectories of particles and the corresponding wall losses.

Author Contributions: Conceptualization, H.-S.C. and J.H.; methodology, H.-S.C.; validation, H.-S.C.; formal analysis, H.-S.C.; investigation, H.-S.C.; resources, J.H.; data curation, H.-S.C.; writing—original draft preparation, H.-S.C.; writing—review and editing, H.-S.C. and J.H.; visualization,

H.-S.C.; supervision, J.H.; project administration, J.H.; funding acquisition, J.H. All authors have read and agreed to the published version of the manuscript.

Funding: This work was supported by a grant from the Subway Fine Dust Reduction Technology Development Project of the Ministry of Land Infrastructure and Transport (21QPPW-B152306-03).

Institutional Review Board Statement: Not applicable.

Informed Consent Statement: Not applicable.

Data Availability Statement: The data presented in this study are available on request from the corresponding author.

Conflicts of Interest: The authors declare no conflict of interest.

References

1. Meng, J.; Liu, J.; Sun, P.; Wan, Y.; Fan, Y.; Xiao, X. Experimental investigation on particle number emission from diesel engine with bipolar discharge coagulation. *Proc. Inst. Mech. Eng. Part D J. Automob. Eng.* **2019**, *233*, 1524–1533. [CrossRef]
2. Bin, H.; Yang, Y.; Cai, L.; Zhulin, Y.; Roszak, S.; Linjun, Y. Experimental study on particles agglomeration by chemical and turbulent agglomeration before electrostatic precipitators. *Powder Technol.* **2018**, *335*, 186–194. [CrossRef]
3. Hautanen, J.; Kilpeläinen, M.; Kauppinen, E.I.; Lehtinen, K.; Jokiniemi, J. Electrical agglomeration of aerosol particles in an alternating electric field. *Aerosol Sci. Technol.* **1995**, *22*, 181–189. [CrossRef]
4. Kim, Y.S.; Lee, J.B.; Hwang, J.; Park, K.S. An experimental study of electrical agglomeration of fine particles in an alternating electric field. In Proceedings of the 7th International Conference on Electrostatic Precipitation, Kyongju, Republic of Korea, 20–25 September 1998.
5. Jaworek, A.; Sobczyk, A.; Marchewicz, A.; Krupa, A.; Czech, T.; Śliwiński, Ł.; Ottawa, A.; Charchalis, A. Two-stage vs. two-field electrostatic precipitator. *J. Electrost.* **2017**, *90*, 106–112. [CrossRef]
6. Chen, H.; Luo, Z.; Jiang, J.; Zhou, D.; Lu, M.; Fang, M.; Cen, K. Effects of simultaneous acoustic and electric fields on removal of fine particles emitted from coal combustion. *Powder Technol.* **2015**, *281*, 12–19. [CrossRef]
7. Sobczyk, A.; Marchewicz, A.; Krupa, A.; Jaworek, A.; Czech, T.; Śliwiński, Ł.; Kluk, D.; Ottawa, A.; Charchalis, A. Enhancement of collection efficiency for fly ash particles (PM2.5) by unipolar agglomerator in two-stage electrostatic precipitator. *Sep. Purif. Technol.* **2017**, *187*, 91–101. [CrossRef]
8. Lehtinen, K.E.J.; Jokiniemi, J.K.; Kauppinen, E.I.; Hautanen, J. Kinematic coagulation of charged droplets in an alternating electric field. *Aerosol Sci. Technol.* **1995**, *23*, 422–430. [CrossRef]
9. Laitinen, A.; Hautanen, J.; Keskinen, J.; Kauppinen, E.; Jokiniemi, J.; Lehtinen, K. Bipolar charged aerosol agglomeration with alternating electric field in laminar gas flow. *J. Electrost.* **1996**, *38*, 303–315. [CrossRef]
10. Kildesø, J.; Bhatia, V.K.; Lind, L.; Johnson, E.; Johansen, A. An experimental investigation for agglomeration of aerosols in alternating electric fields. *Aerosol Sci. Technol.* **1995**, *23*, 603–610. [CrossRef]
11. Ji, J.-H.; Hwang, J.; Bae, G.-N.; Kim, Y.-G. Particle charging and agglomeration in DC and AC electric fields. *J. Electrost.* **2004**, *61*, 57–68. [CrossRef]
12. Choi, H.S.; Hwang, J. Reduction of submicron-sized aerosols emission in electrostatic precipitation by electrical attraction with micron-sized aerosols. *Powder Technol.* **2021**, *377*, 882–889. [CrossRef]
13. Sun, Z.; Yang, L.; Shen, A.; Zhou, L.; Wu, H. Combined effect of chemical and turbulent agglomeration on improving the removal of fine particles by different coupling mode. *Powder Technol.* **2019**, *344*, 242–250. [CrossRef]
14. Chen, D.; Wu, K.; Mi, J. Experimental investigation of aerodynamic agglomeration of fine ash particles from a 330 MW PC-fired boiler. *Fuel* **2016**, *165*, 86–93. [CrossRef]
15. Liu, H.; Yang, F.; Tan, H.; Li, Z.; Feng, P.; Du, Y. Experimental and numerical investigation on the structure characteristics of vortex generators affecting particle agglomeration. *Powder Technol.* **2020**, *362*, 805–816. [CrossRef]
16. Crynack, R.; Truce, R.; Harrison, W. Indigo particle agglomerators reduce mass and visible emissions on coal fired boilers in the US. In Proceedings of the 10th International Conference of Electrostatic Precipitator, Cairns, Australia, 26–30 June 2006.
17. Truce, R.; Wilkins, J.; Crynack, R.; Harrison, W. Enhanced fine particle collection using the indigo agglomerator. In Proceedings of the 10th International Conference of Electrostatic Precipitator, Cairns, Australia, 26–30 June 2006.
18. Singh, M.; Singh, R.; Singh, S.; Walker, G.; Matsoukas, T. Discrete finite volume approach for multidimensional agglomeration population balance equation on unstructured grid. *Powder Technol.* **2020**, *376*, 229–240. [CrossRef]
19. Koizumi, Y.; Kawamura, M.; Tochikubo, F.; Watanabe, T. Estimation of the agglomeration coefficient of bipolar-charged aerosol particles. *J. Electrost.* **2000**, *48*, 93–101. [CrossRef]
20. Tan, B.; Wang, L.; Wu, Z. An approximate expression for the coagulation coefficient of bipolarly charged particles in an alternating electric field. *J. Aerosol Sci.* **2008**, *39*, 793–800. [CrossRef]
21. Saffman, P.G.; Turner, J.S. On the collision of drops in turbulent clouds. *J. Fluid Mech.* **1956**, *1*, 16–30. [CrossRef]
22. Higashitani, K.; Yamauchi, K.; Matsuno, Y.; Hosokawa, G. Turbulent coagulation of particles dispersed in a viscous fluid. *J. Chem. Eng. Jpn.* **1983**, *16*, 299–304. [CrossRef]

23. Alves, A.; Paiva, J.; Salcedo, R. Cyclone optimization including particle clustering. *Powder Technol.* **2015**, *272*, 14–22. [CrossRef]
24. Wang, L.K. *Advanced Air and Noise Pollution Control*; Humana: Totowa, NJ, USA, 2005.
25. Wang, J.; Huang, W.; Xu, H.; Wang, H.; Ding, Y.; Qu, Z.; Yan, N. Charged movement characteristics and enhanced removal of fine particles under the electric fields coupling with turbulence from industrial flue gas. *Fuel* **2022**, *326*, 124977. [CrossRef]